THE INTERNATIONAL JOURNAL OF SCIENCE & TECHNOLEDGE

Photocurrent Calculations in Magnetic Solids by using Relativistic Kronig-Penney Model

Lalnunpuia
Research Scholar, Department of Physics, Mizoram University, Aizawl, Mizoram, India
Aldrin Malsawmtluanga
Research Scholar, Department of Physics, Mizoram University, Aizawl, Mizoram, India
Lawrence Z. Chhangte
Research Scholar, Department of Physics, Mizoram University, Aizawl, Mizoram, India
Ricky L. Ralte
Research Scholar, Department of Physics, Mizoram University, Aizawl, Mizoram, India
Z. Pachuau
Professor, Department of Physics, Mizoram University, Aizawl, Mizoram, India

Abstract: Relativistic Kronig-Penney (RKP) model have been used for the photoemission calculations from magnetic solids like Fe, Ni, Cr and W. For the evaluation photocurrent the initial wavefunction used is the modified form of Davison and Steslicka. Spatially dependent vector potential had been used to evaluate the relevant matrix elements.

Keywords: Photoemission, relativistic kronig-penney model, dirac equation, wavefunction, magnetic solids

1. Introduction

Kronig-Penney(KP) model has then been used for the calculations of surface electronic states by several authors (Statz, 1950; Tamm, 1932; Schockley, 1939; Davison and Levine, 1970; Thapa, 1993). Schaich and Ashcroft (1971) have calculated numerically the photo yield by using the modified form of the K-P model. Steslicka(1974) had done detailed calculations of the surface states using the Kronig-Penney model both for the semi-infinite and infinite crystals. Eldib *et al.*(1987) has also applied the K-P model to one dimensional crystal. They calculated only the electronic energy bands for mono and poly-atomic crystals and compared the data with the one computed using Linear combination of atomic orbitals (LCAO) method. Thapa and Kar (1988, 1995) have also developed ψ_i by using Kronig-Penny model, and used it for photo-emission calculations.

It has been seen that most of the authors (Das *et al.,* 1991; Thapa *et al.,*1994; Pachuau *et al.,*1999; Thapa and Kar, 1995) have not taken into consideration the effect of relativity while applying the Kronig-Penney (KP) model to the band structure studies in metals like W, Si, Al, Pd, etc. In their studies, the relativistic effect on the motion of the electron in the potential well was not taken into consideration while deriving the initial state wave function ψ_i of the electron. A detailed energy band calculations using relativistic Kronig-Penney(RKP) have been done by Davison and Steslicka (DS) (1969) by solving the Dirac equation for bulk spinors for which the surface state calculations were also given. In this paper, we are discussing a simple relativistic approach to photo-emission study by using the wave function as deduced by DS.

In this paper, we will discuss the crystal potential of the solid which is represented by the Kronig-Penney potential and Dirac equation will be solved to obtain the initial wave functions. We have considered the variations of the dielectric functions for the calculations of the photon fields, but adopted the wave functions for the initial state of the electrons as developed by Davison and Steslicka (DS). We have introduced the surface of width 'd' into the potential model and used the wave functions for the evaluation of the matrix elements for photocurrent calculations.

2. Formalism

In three-dimensional Dirac theory, the particle is found to have *intrinsic spin,* which is fundamentally connected to the orbital angular momentum of the particle. In one-dimension, there is no analogue to orbital angular momentum; hence, there need be no intrinsic spin. In the following, we will deal only with the one-dimensional Dirac equation neglecting the spin-orbit interaction term, for simplicity.

For a linear crystal with a clean surface, the potential field is assumed to be of the form shown in figure 1. The periodicity of the lattice is n(a+b), n being integer and (a+b) the lattice constant. The potential inside the crystal is represented by a periodic array of rectangular

wells of depth V_3, which is subsequently taken to infinity, in such away that $\begin{array}{c} Lim \; V_3 b = a_0 \\ V_3 \to \infty \\ b \to 0 \end{array}$, where b is the width of the potential

barrier and a_0 is a positive arbitrary constant. The crystal surface potential is $V_1 > \varepsilon_0$ where ε_0 is the kinetic energy related to the

energy (E) of the electron by the relation $E = \varepsilon_0 + m_0 c^2$, m_O being the rest mass of the electron. In the K-region of constant potential

V_k, the two component form of the one-dimensional time-independent Dirac equation can be written as,

$$ihc\frac{d\phi_k^{(1)}}{dx} = (\varepsilon_0 - V_k)\phi_k^{(2)}$$

$$ihc\frac{d\phi_k^{(2)}}{dx} = \left\{ (\varepsilon_0 - V_k) + 2m_0 c^2 \right\} \phi_k^{(1)}$$

(1)

c is the velocity of light.

Decoupling the above two equations to obtain
$$\frac{d^2 \phi_k^{(j)}}{dx^2} = -\rho_k^2 \phi_k^{(j)} \qquad j = 1, 2 \qquad (2)$$

where $\qquad \rho_k^2 = \dfrac{(\varepsilon_0 - V_k)[(\varepsilon_0 - V_k) + 2m_0 c^2]}{\hbar^2 c^2}$

(3)
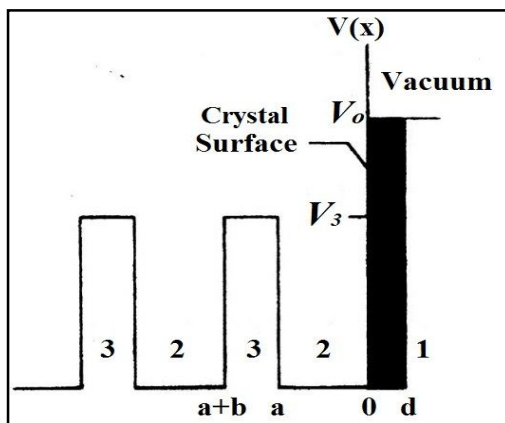
Figure 1: Schematic representation of a semi-infinite one-dimensional crystal potential field with a surface   potential of $V_1 > \varepsilon_0$
(modified form of Davison and Stelicska, 1969).

The plane wave solution of Eq. (2) for bulk and vacuum regions can be written as:

$$\psi_i(x) = \begin{cases} \varphi_2(x) = \alpha_2^{(2)}\left[\begin{pmatrix} -\gamma_2 \\ 1 \end{pmatrix} e^{i\rho_2 x} + \lambda \begin{pmatrix} \gamma_2 \\ 1 \end{pmatrix} e^{-i\rho_2 x} \right], & bulk \\ \varphi_1(x) = \begin{pmatrix} \gamma_1 \\ 1 \end{pmatrix} \beta_1^{(2)} l_1 x , & vacuum \end{cases}$$

(4)

where $l_1 = -i\rho_1 > 0$ and is real. The constants in Eq. (4) are defined as

$$E = \varepsilon_0 + m_0 c^2, \qquad \alpha_k^{(1)} = -\gamma_k \alpha_k^{(2)}, \qquad \beta_k^{(1)} = \gamma_k \beta_k^{(2)}$$

$$\gamma_k = \frac{\varepsilon_0 - V_k}{hc\rho_k} \quad \text{and} \quad \lambda = \frac{\beta_2^{(2)}}{\alpha_2^{(2)}} = \frac{1 - e^{i(\rho_2 - \mu)a}}{e^{-i(\rho_2 + \mu)a} - 1}$$

(5)

μ is the wave number and is given by $\mu = \dfrac{n\pi}{a} + i\zeta$ where ζ is real and $\zeta > 0$.

To compute the photon field, we have used the simple model of Bagchi and Kar (1978). With simple modification the photon field used in our calculation can be written as

$$\tilde{A}_\omega(z) = \begin{cases} A_1, & (bulk) \\ \dfrac{A_1 . \varepsilon(\omega).d}{[1-\varepsilon(\omega)]z + d} , & (surface) \\ A_1 . \varepsilon(\omega), & (vacuum) \end{cases}$$

(6)

where A_1 is a constant depending on the dielectric function $\varepsilon(\omega)$, photon energy $\hbar\omega$ and angle of incidence θ_i.

The final state wave function ψ_f is the scattering state (Bagchi and Kar, 1978) of the step potential defined by $V(x) = -V_0\theta(x)$, where $\theta(x)$ is unit function which is encountered by the electron, and is given by (in atomic units)

$$\psi_f(z) = \begin{cases} \left(\dfrac{1}{2\pi q_f}\right)^{\frac{1}{2}} \dfrac{2q_f}{q_f + k_f} e^{ik_f z} e^{-\alpha|z|} & z \leq 0 \\[3mm] \left(\dfrac{1}{2\pi q_f}\right)^{\frac{1}{2}} \left(e^{iq_f z} + \dfrac{q_f - k_f}{q_f + k_f}\right) e^{-iq_f z} & z \geq 0 \end{cases} \qquad (7)$$

where $k_f^2 = 2E_f$, $q_f^2 = 2(E_f - V_0)$ and $E_f = E_i + \hbar\omega$,

The factor $e^{-\alpha|x|}$ is included on the bulk and surface side to take into account the inelastic scattering of the electrons.

Using the final state wave function ψ_f as the scattering state of the step potential at x = 0 and photon field vector of Eq. (6), the photocurrent density is calculated by using the Fermi golden rule formula (Penn, 1972) as

$$\frac{d\,j(E)}{d\Omega} = \frac{2\pi}{h} \sum_f \left| \langle \psi_f | H^I | \psi_i \rangle \right|^2 \delta(E - E_f) \delta(E_f - E_i - \hbar\omega) f_o(E - \hbar\omega) \left[1 - f_o(E)\right] \qquad (8)$$

Here the perturbation H^I is given by

$$H^I = \frac{e}{2m_e c}(\mathbf{p}.\mathbf{A} + \mathbf{A}.\mathbf{p}) \qquad (9)$$

where $\mathbf{p}$ is a one-electron momentum operator and $\mathbf{A}$ is the vector potential. $\mathbf{A}$ is assumed to be a constant in the bulk and vacuum regions, but in the surface region, it is a function of x being the solution of Maxwell's equation for dielectric function $\epsilon(x)$.

The matrix element $\langle \psi_f | H^I | \psi_i \rangle$ involved in Eq. (9) can be written as the following for calculating the photocurrent:

$$I = \langle \psi_f | H^I | \psi_i \rangle = \int_{-\infty}^{\infty} \psi_f^* H^I \psi_i dz = \int_{-\infty}^{\infty} \psi_f^* \left(\tilde{A}_\omega(z)\frac{d}{dz} + \frac{1}{2}\frac{d}{dz}\tilde{A}_\omega(z)\right)\psi_i\,dz \qquad (10)$$

Since the integrals in the matrix element cannot be solved analytically, FORTRAN programs are developed to evaluate for computing photocurrent as a function of photon energy.

Photocurrent was calculated as a function of photon energy ($\hbar\omega$) by evaluating the integrals in Eq. (10). The formalism was then applied to the case of magnetic solids like Cr, Fe, Ni and W. For these metals, we have used the experimentally determined dielectric functions $\varepsilon(\omega)$ (Lide, 2004; Palik, 1991) and our generated data (using WIEN2k code developed by Blaha *et al.,* 2008). Since our calculation is purely a model type, we used the same value of the following data (in atomic units):

Fermi energy (E_F) = 0.3768, Potential strength (V_O) = 0.5514,

Work function (Φ) = 0.1746, Potential width (a) = $6\,a_o$ (a_o = Bohr radius)

Velocity of light(c) = 137, Surface width (d) = 10

The relativistic parameters used in the calculations are given by :

$\rho_1 = i0.59093$, $\rho_2 = 0.868106$, $l_1 = 0.590930$

$\gamma_1 = -i0.000753$, $\gamma_2 = 0.002388$, $\eta = 6\times10^{-4}$

The values of RKP parameters like β_1, β_2, α_1, α_2 and λ were calculated for band index number $n=10$. These values were substituted into the matrix element *I* for the evaluation of photocurrent.

3. Results and Discussion

We discuss here the results of photocurrent in the case of magnetic solids using the experimentally measured dielectric constants and generated data for the calculation of photocurrent against the incident photon energy ($\hbar\omega$). The angle of incidence was $\theta_i = 45^0$ for *p*-polarised light under consideration in all the cases.

3.1. Molybdenum and Tungsten

Photocurrent was calculated for these metals using surface widths $a = 10$ a.u. for the same values of surface state energy (10.24 eV), same potential barrier height (14.99 eV) and $\theta_i = 45^0$. Figure 2 shows the plot of photocurrent as a function of photon energy ($\hbar\omega$) in the case of Mo, using experimental data (Lide, 2004) and calculated data of dielectric constants. In the case of experimental data (figure 2a), we find that a maxima in the value of photocurrent occurred at $\hbar\omega = 12$ eV. With further increase of the photon energy, the photocurrent decreased to a minimum value at $\hbar\omega = 20$ eV and then showed another peak of larger amplitude at $\hbar\omega = 27$ eV.

Figure 2(b) shows the plot of variation of photocurrent as a function of photon energy in the case of Mo using Generated data. Here we have almost the same nature as in the case of experimental data, having a small peak at $\hbar\omega = 12.1$eV and decreased to minimum at

photon energy $\hbar\omega$ = 20.5 eV. A second peak is also seen $\hbar\omega$ = 27.6 eV which is having minimum at 34 eV. In both the cases, we have peaks below plasmon energy and above which is larger in height. Plasmon energy of Mo is 25.2 eV (Egerton, 2011). The occurrence of peaks for $\hbar\omega < \hbar\omega_p$ in the photoemission (low frequency regime) is basically a phenomenon occurring due to the spatial variation of the photon field vector, which has already been established experimentally by Levinson *et al.* (1979) and Weng *et al.* (1978).

Figure 3 shows the plot of photocurrent as a function of photon energy ($\hbar\omega$) in the case of W using experimental data (Lide, 2004) and generated data of dielectric constants. In the case of experimental data (figure 3a), we find that a maxima in the value of photocurrent occurred at $\hbar\omega$ = 13.2 eV. With further increase in the photon energy, the photocurrent decreased to a minimum value at $\hbar\omega$ = 20.8 eV and then showed another peak of larger amplitude at $\hbar\omega$ = 28 eV.

Figure 3(b) shows the plot of variation of photocurrent as a function of photon energy in the case of W using generated data. Here we have almost the same nature as in the case of experimental data, having small peak at $\hbar\omega$ = 13.5 eV and decreased to minimum at 21.6 eV photon energy. A second peak is also seen $\hbar\omega$ = 27.6 eV which is having minimum at around 38 eV, the magnitude of second peak is almost four times the first. In both the cases, we have peaks below plasmon energy and above which is larger in height. Plasmon energy of W is 25.2 eV (Oleshko *et al.*, 2002). The occurrence of peaks for $\hbar\omega < \hbar\omega_p$ in the photoemission(low frequency regime) is basically a phenomenon occurring due to the spatial variation of the photon field vector, which has already been established experimentally by Levinson *et al.* (1979) and Weng *et al.* (1978).

We find that both metals Mo and W have shown at least the qualitative features with the behavior of photocurrent as indicated also by other metals like Pd (Thapa, 1993), W (Thapa and Kar, 1994), etc. in which the Kronig-Penney potential model was used. It is obvious that the variation of the vector potential which mainly monitors the matrix element, thereby bringing in the changes in photocurrent. This fact had also been discussed by Weng *et al.* (1978) that the causes in the occurrence of peak in photoemission intensity for Mo is due to excitation of electrons by A_z component of the vector potential perpendicular to surface plane. He further pointed out that the initial states with Δ_1 symmetry can only be photo excited by A_z component of the incident photon field.
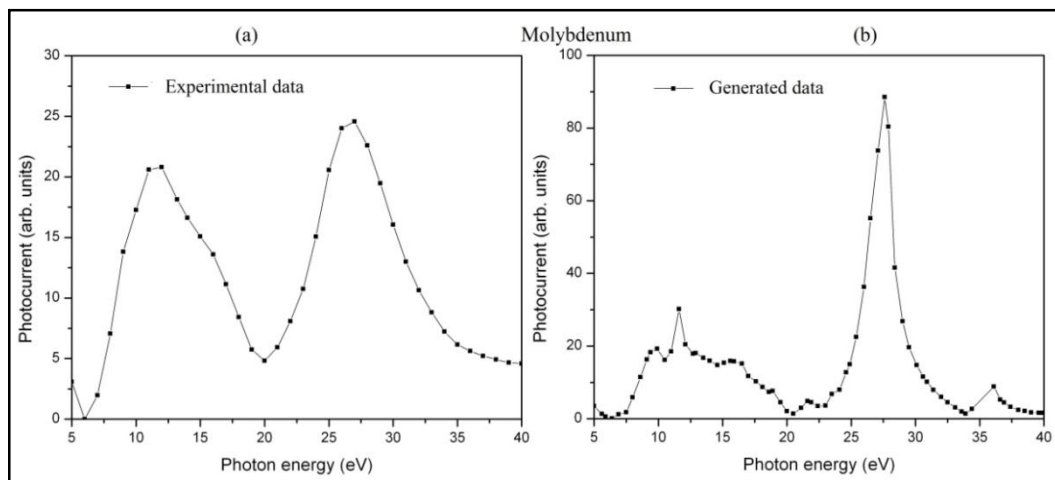
Figure 2: Plot of photocurrent against the photon energy $\hbar\omega$ for Mo, using relativistic KP model.
(a) Experimental data and (b) Generated data
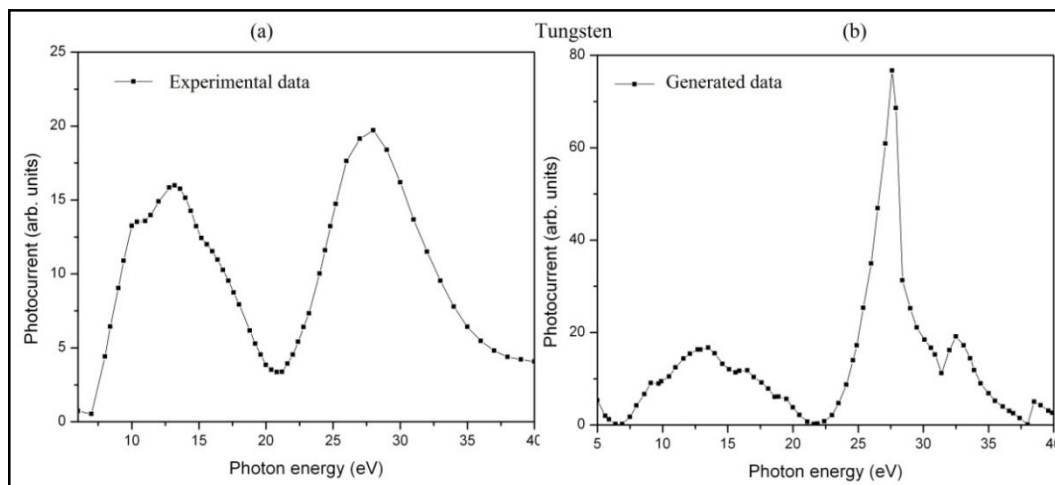
Figure 3: Plot of photocurrent against the photon energy $\hbar\omega$ for W using relativistic KP model.
(a) Experimental data and (b) Generated data

3.2. Iron and Nickel

Photocurrent was calculated for these metals for the values of the surface widths a = 10 a.u. for the same values of surface state energy (10.24 eV), potential barrier height (14.99 eV) and $\theta_i = 45^0$. Figure 4 shows the plot of photocurrent as a function of photon energy ($\hbar\omega$) in the case of Fe using experimental data (Lide, 2004) and generated data of dielectric constants. In the case of experimental data (figure 4a), we find that a maxima in the value of photocurrent occurred at $\hbar\omega$ = 11 eV. With further increase of the photon energy, the photocurrent decreased to a minimum value at $\hbar\omega$ = 16 eV and then increase to a maximum peak of larger amplitude at $\hbar\omega$ = 24.5 eV. Figure 4(b) shows the plot of variation of photocurrent as a function of photon energy in the case of Fe using calculate data. Here we have almost the same nature as in the case of experimental data, having small peak at $\hbar\omega$ = 1.6 eV and decreased to minimum at 16 eV photon energy. A second peak is also seen $\hbar\omega$ = 19.6 eV which is having minimum at 25.4 eV which is closed to the plasmon energy 25.2 eV (Oleshko et al., 2002). Third peak having a magnitude much lager than the first two peak is observed at 32.5 eV.

Nickel is an interesting transition metal to study with spin- and angle-resolved photoemission because the electronic structure part of the calculation causes the calculate results to differ drastically from the experimental ones (Himpsel et al., 1979).

Figure 5 shows the plot of photocurrent as a function of photon energy ($\hbar\omega$) in the case of Ni using experimental data (Lide, 2004) and generated data of dielectric constants. In the case of experimental data (figure 5a), we find that a maxima in the value of photocurrent occurred at photon energy $\hbar\omega$ = 12 eV. With further increase in the photon energy, the photocurrent decreased to 16 eV and then it increases again showing peak of larger amplitude at around $\hbar\omega$ = 23 eV.
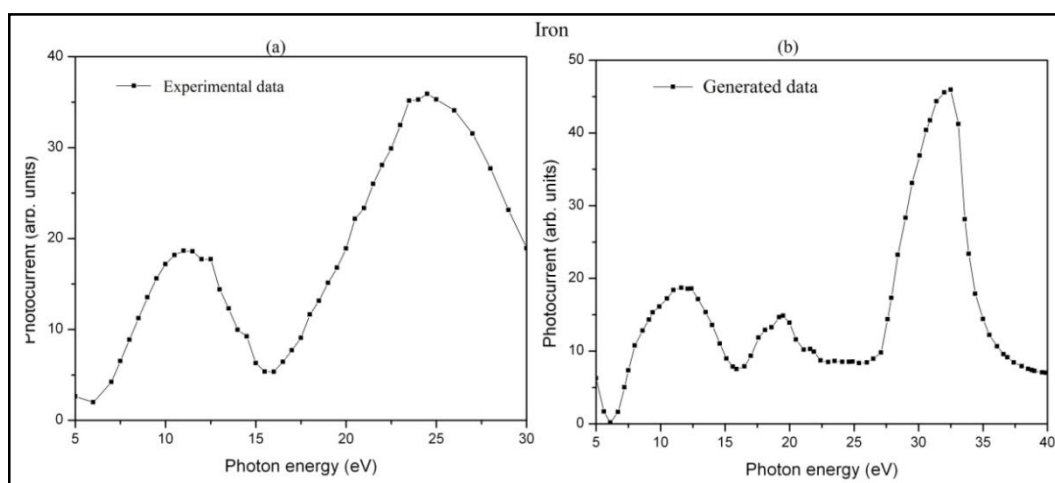
Figure 4: Plot of photocurrent against the photon energy $\hbar\omega$ for Fe using the relativistic KP model.
(a) Experimental data and (b) Generated data

Figure 5(b) shows the plot of variation of photocurrent as a function of photon energy in the case of Ni using calculate data. Here the nature of the graph is same below photon energy 25 eV. The first minimum is observer at 17.5 eV, whereas the second minimum is at 27.5 eV. A third peak having a larger amplitude with compare to the first two is observed around 34 eV, but showed no clear minimum. In the case of experimental data and generated data peaks are observed around plasmon energy $\hbar\omega$ = 25 eV (Moneta and Pawlowski, 2005; Oleshko et al., 2002).
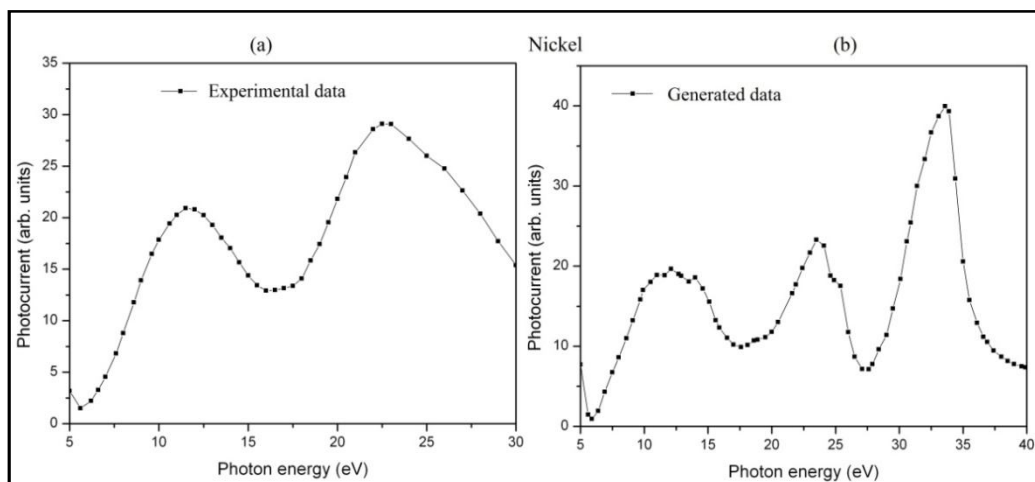
Figure 5: Plot of photocurrent against the photon energy $\hbar\omega$ for Ni using the relativistic KP model.
(a) Experimental data and (b) Generated data

4. Conclusion

Though the model used is simple, this type of calculations gives first hand information with regard to photoemission. However, there are shortcomings in the formalism developed. For example, we have used the same wavefunction both for the surface and the bulk region of the solids. Also, it is the spatial variation of the photon fields which is monitoring the changed in photocurrent. For more accurate results, it would be appropriated if one can extend such type of calculation by incorporating relativistic wavefunctions as well as for the vector potential.

5. References

i. Statz H. Z. Naturforsch, 5A: 534, 1950
ii. Tamm Ig., Some remark on the Theory of Photoelectric Effect on Metals. Phys. Rev. 39: 170-172,1932
iii. Schockley W. On the Surface States Associated with a Periodic Potential. Phys. Rev., 56: 317-323, 1939
iv. Davison S.G. and Levine J.D. Surf. States. Sol. Stat. Phys., 25: 1-149, 1970
v. Thapa R.K. Photoemission calculation using Kronig-Penney model and spatially dependent vector potential: Application to Pd. Phys. Stat. Sol., B179: 391-397, 1993
vi. Schaich W.L. and Ashcroft N.W. Model Calculations in the Theory of Photoemission, Phys. Rev., B3: 2452-2465, 1971
vii. Steslicka M. Kronig-Penney model for surface states. Prog. Surf. Sci., 5: 157-259, 1974
viii. Eldib A.M., Hasson H.F. and Mohmad M.A. J. Phys., C20: 3011, 1987
ix. Thapa R.K. and Kar N. Photoemission calculation from band state using Kronig-Penney model and spatially varying photn field. Indian J. Pure and Appl Phys., 26: 620-623, 1988
x. Thapa R.K. and Kar N. Kronig-Penney model treatment of photoemission from silicon. Surf. Sci., 338: 138-142, 1995
xi. Das P., Thapa R.K. and Kar N. Photoemission calculation with a simple model for the photon field: Application to alluminium. Mod. Phys. Lett., B5: 65-72, 1991
xii. Thapa R.K., Das P. and Kar N. Photoemission calculation with Kronig-Penney model. Mod. Phys. Lett., B8: 361-366, 1994
xiii. Pachuau Z., Gurung S., Thapa R.K., Khating D.T. and Kar N. Photocurrent Calculations in Semiconductor using Kronig-Penney model. Indian J. Phys., 73A: 237-243, 1999
xiv. Davison S.G. and Steslicka M. Relativistic theory of Tamm surface states. J. Phys. (Sol. Stat. Phys.), C2: 1802 , 1969
xv. Bagchi A. and Kar N. Refraction effects in angle-resolved photoemission from surface states on metals. Phys. Rev., B18: 5240-5247, 1978
xvi. Penn D.R. (Photoemission spectroscopy in the presence of adsorbate-covered surfaces, Phys. Rev. Lett., 28: 1041-1044 , 1972.
xvii. Palik E.D. (ed.). Handbook of Optical Constants of Solids. Academic Press, 1991
xviii. Lide D.R. (ed.). Handbook of Chemistry and Physics. 84 Ed., CRC Press, 2004
xix. Blaha P., Schwarz K., Madsen G.K.H., Kvasnicka D. and Luitz J. WIEN2k, An Augmented Plane Wave + Local Orbitals Program for Calculating Crystal Properties (Karlheinz Schwarz, Techn. Universitat Wien, Austria), ISBN 3-9501031-1-2, 2008
xx. Egerton R.F. Electron Energy-Loss Spectroscopy in the Electron Microscope. Springer Science Business Media, LLC, NY, 3rd Ed, 2011.
xxi. Levinson H.J., Plummer E.W. and Feibelman P.J. Effects on Photoemission of the Spatially Varying Photon Field at a Metal Surface. Phys. Rev. Lett., 43: 952-955, 1979.
xxii. Weng S.L, Gustaffson T. and Plummer E.W. Experimental and theoretical study of the surface resonances on the (100) faces of W and Mo. Phys Rev., B18: 1718-1739, 1978.
xxiii. Oleshko V.P., Murayama M., and Howe J. M. Use of Plasmon Spectroscopy to Evaluate the Mechanical Properties of Materials at the Nanoscale. Microsc. Microanal. 8: 350–364, 2002
xxiv. Himpsel F.J., Knapp J.A. and Eastman D.E. Experimental energy-band dispersions and exchange splitting for Ni. Phys. Rev., B19 2919-2927, 1979
xxv. Moneta M. and Pawowski B.. Ion stopping cross-section at ferro-paramagnetic phase transition. Vacuum, 78: 467-472, 2005